

Unravelling spontaneous Bloch-type skyrmion in centrosymmetric two-dimensional magnets

Jingman Pang², Xiaohang Niu¹, Hong Jian Zhao³, Yun Zhang^{1*}, Laurent Bellaiche⁴

¹ *College of Physics and Optoelectronic Technology, Collaborative Innovation Center of Rare-Earth Functional Materials and Devices Development, Baoji University of Arts and Sciences, Baoji 721016, China*

² *Faculty of Chemistry and Chemical Engineering, Baoji University of Arts and Sciences, 1 Hi-Tech Avenue, Baoji, Shaanxi, P. R. China*

³ *Key Laboratory of Material Simulation Methods and Software of Ministry of Education, College of Physics, Jilin University, Changchun 130012, China*

⁴ *Physics Department and Institute for Nanoscience and Engineering, University of Arkansas, Fayetteville, Arkansas 72701, USA*

*E-mail: zhangyun_xtu@163.com

Keywords: two-dimensional magnets, magnetic skyrmions, first-principle calculation

Abstract:

The realization of magnetic skyrmions in two-dimensional (2D) magnets holds great promise for both fundamental research and device applications. Despite recent progress, two-dimensional skyrmions hosts are still limited, due to the fact that most 2D magnets are centrosymmetric and thus lack Dzyaloshinskii–Moriya interaction (DMI). We show here, using a general analysis based on symmetry, that Bloch-type skyrmions can, in fact, be stabilized in 2D magnets, due to the interplay between in-plane component (d_x) of second nearest-neighbor DMI and magnetic anisotropy. Its validity is demonstrated in $\text{Cr}_2\text{Ge}_2\text{Te}_6$ monolayer, which is also verified by recent experiments. Our work gives a clear direction for experimental studies of 2D magnetic materials to stabilize skyrmions and should greatly enrich the research on magnetic skyrmions in 2D lattices.

Introduction

Magnetic skyrmions are a special class of vortex- or antivortex-like noncollinear spin textures [1-3]. Such spin textures showcase a variety of intriguing features (e.g., compact size, topological stability, and low-threshold driven currents), enabling the design of high-performance information processing and storage devices [4]. In principle, magnetic skyrmions provide a promising pathway to perpetuating the Moore's law [5]. Since its first realization in cubic B20 MnSi, the quest for magnetic skyrmions has received renewed interest. To date, magnetic skyrmions were experimentally discovered or theoretically proposed in a variety of materials, including bulk magnets and synthetic multilayer films composed of magnetic and heavy-metal layers [6-18]. In most cases, magnetic skyrmions are induced by chiral interactions between atomic spins, known as Dzyaloshinskii-Moriya interaction (DMI) [19, 20], existing in non-centrosymmetric magnetic compounds or in thin films in which inversion symmetry is broken by the presence of an interface [21].

In the past few years, magnetism in low dimensions has received renewed interest, marked by the observation of long-range magnetic order in 2D van der Waals materials, including but not limited to CrI₃, CrGeTe₃, and Fe₃GeTe₂ [22-24]. This offers a promising alternative avenue for exploring exotic topological spin phenomena. Of particular interest, the Bloch-type magnetic skyrmions/bubbles have been very recently observed in van der Waals Cr₂Ge₂Te₆ [25-29]. However, the occurrence of skyrmions in this system goes against expectations due to that fact that its crystal structure is centrosymmetric with a honeycomb lattice, thereby precluding the manifestation of DMI. The intrinsic origin of topological spin textures in centrosymmetric van der Waals magnets like Cr₂Ge₂Te₆ remains elusive [26, 30]. Apart from Cr₂Ge₂Te₆, there are many 2D magnetic materials that share the similar structure, while most of them exhibit collinear magnetic structure. Therefore, exploring alternative mechanisms to realize skyrmions in a new category of centrosymmetric materials will significantly enrich the diversity of magnetic skyrmion materials.

In the present work, we unveil that skyrmions can be spontaneously stabilized in centrosymmetric 2D magnets with a honeycomb lattice. Based the symmetry analysis, we demonstrate that centrosymmetric 2D magnets with a honeycomb lattice exhibit

finite second NN DMI due to the broken *local* inversion symmetry, which is primarily responsible for the formation of skyrmions. By using first-principles calculations and Monte Carlo simulations, we reproduce the spin spiral and skyrmions phases experimentally observed in $\text{Cr}_2\text{Ge}_2\text{Te}_6$. This unusual skyrmionics physics is revealed by introducing the dimensionless parameter κ , which can serve as a measurement whether the ground state is a non-collinear magnetic structure or not. Furthermore, we present the anisotropy-field phase diagram. Furthermore, we present the anisotropy-field phase diagram, demonstrating that not only out-of-plane anisotropy but also in-plane anisotropy favors the formation of skyrmionic states.

Results and discussion

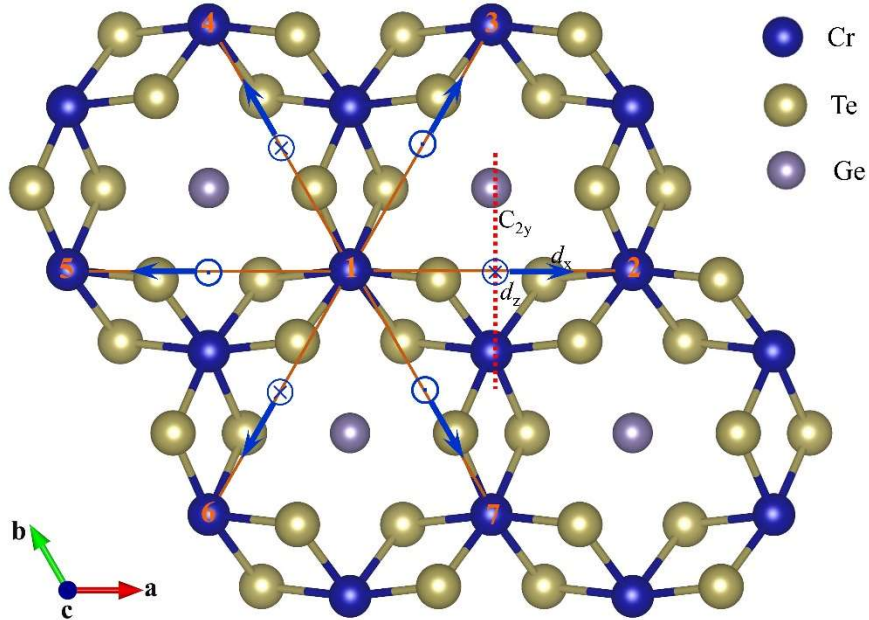


Figure 1. Structure of monolayer $\text{Cr}_2\text{Ge}_2\text{Te}_6$. (a, b, c) are the crystallographic directions and a is along x direction and c along z direction of Cartesian coordinates.

Let us first consider the crystal structure of monolayer $\text{Cr}_2\text{Ge}_2\text{Te}_6$, as illustrated in Figure 1. The crystal adopts the space group $\bar{P}31m$. Obviously, monolayer $\text{Cr}_2\text{Ge}_2\text{Te}_6$ presents overall inversion symmetry, and thus the DMI between the first nearest neighbors (NN) will cancel out upon space inversion, in accordance with Moriya's first rule [20]. However, it is noteworthy that local inversion symmetry is inherently broken for the second nearest neighbors. Let's take Cr_1 - Cr_2 pair as an example. As indicated in Figure 1, there is a two-fold rotation axis C_{2y} perpendicular to the line connecting the second NN. According to Moriya's fourth rule [20], the DM vector is perpendicular to

this axis. Consequently, the DM vector associated with Cr₁-Cr₂ pair possesses a z component (d_z) and a planar component (d_x) aligned along Cr₁-Cr₂ bond. Considering the three-fold rotational symmetry around [001] and the translational symmetry, the in-plane component of the DM vector between Cr₁ and Cr_{*i*} ($i = 2-7$) points towards (or away from) Cr₁. While the out-of-plane component alternates in sign every 60 degrees, specifically, the orientation of d_z component remains consistent for Cr₁-Cr₂, Cr₁-Cr₄, and Cr₁-Cr₆ pairs, which is opposite to that of the Cr₁-Cr₃, Cr₁-Cr₅, and Cr₁-Cr₇ pairs.

Based on the symmetry analysis presented above, we demonstrate that a finite second NN DMI is allowed to exist in centrosymmetric 2D magnetic materials with a honeycomb lattice owing to the broken local inversion symmetry. Usually, the ratio of first NN DMI (d_1) to the J_1 is regarded as an important parameter to assess the feasibility of forming topological spin textures. The typical range for $|d_1/J_1|$ falls within 0.1–0.2 [31]. However, for monolayer Cr₂Ge₂Te₆ and other 2D magnetic materials with similar structure, the d_1 is inhibited by inversion symmetry. To deeply understand this unusual skyrmionics physics in centrosymmetric 2D magnetic materials with a honeycomb lattice, we thus introduce the dimensionless parameter $\kappa = \left(\frac{4}{\pi}\right)^2 \frac{AK}{D^2}$, that can help us identify magnetic ground state [32, 33]. Here A is the exchange stiffness that includes both Heisenberg exchange interaction J_1 and J_2 , K is the total magnetic anisotropy, and D is the DMI parameter in micromagnetic format, respectively. It has been demonstrated that, when $0 < \kappa < 1$, the magnetic ground state of the system exhibits spin spiral. Under a moderate magnetic field, spin spiral might transform into skyrmions. Whereas for $\kappa > 1$, the system tends to exhibit a collinear magnetic structure, i.e., a FM state.

The material parameter A is related to the parameters of the atomistic model by:

$$A = \frac{1}{2V} \sum_j J_{0j} (R_{0j}^x)^2 = \frac{a^2}{2V} \left(\frac{1}{2} J_1 + 3J_2 \right) \quad (1)$$

Here J_{0j} is the NN and second NN Heisenberg exchange interactions, R_{0j}^x is the x component of Cr pair vector, respectively. V is the volume of the magnetic part of the unit cell, e.g. the Cr₂Ge₂Te₆ monolayer. And a is the distance between two second NN

Cr atoms. As indicated by our symmetry analysis, the orientation of d_z for adjacent second NNs is opposite for centrosymmetric 2D magnetic materials with a honeycomb lattice, thus only the d_x is left to contribute to the material parameter D . Hence, D can be expressed as follow:

$$D = \frac{1}{V} \sum_j d_{0j}^x R_{0j}^x = \frac{a}{V} (3d_2^x) \quad (2)$$

Finally, we can rewrite κ with the parameters of atomistic model as:

$$\kappa = \left(\frac{4}{\pi}\right)^2 \frac{(J_1 + 6J_2)K}{(6d_2^x)^2} \quad (3)$$

We now examine the SIA- d_x phase diagram at 0 K without external magnetic field. To this end, we adopt the following spin Hamiltonian in parallel tempering Monte Carlo (PTMC) simulations:

$$H = -\frac{1}{2} \sum_{\langle i,j \rangle} J_{ij} \mathbf{S}_i \cdot \mathbf{S}_j - \frac{1}{2} \sum_{\langle i,j \rangle} \mathbf{d}_{ij}^x \cdot (\mathbf{S}_i \times \mathbf{S}_j) - \sum_i K (S_i^z)^2 - B \sum_i S_i^z \quad (4)$$

here \mathbf{S}_i is the unit vector of spin at site i . The isotropic Heisenberg exchange coupling, denoted by J_{ij} , spans over all first and second nearest-neighbor (NN) magnetic ions. Second term \mathbf{d}_{ij}^x represents the vector that characterizes the x component of DMI for the second NN magnetic ions. The third term is the single ion anisotropy K . In the last term, B indicates the strength of the external magnetic field along Z axis, which is same as indicting in Figure 1. The PTMC simulations are performed over a $60 \times 60 \times 1$ supercell. The phase diagram is obtained by fixing $J_1 = 10$ meV and $J_2 = 0$ meV as a function of the d_x and single ion anisotropy (SIA). To obtain the ground state at 0 K, various periods of spin spirals are inputted as initial states for each set of magnetic parameters and fully relax them. The energy of the FM state (FM-x for easy-plane anisotropy, and FM-z for easy-axis anisotropy) is set as the zero reference. One can clearly see in Figure 2 that, within the $|\kappa| < 1$ threshold, the spin spiral is indeed more energetically favorable compared to FM state for both easy-axis and easy-plane anisotropy. Even a small second NN d_x , when coupled with sufficiently low SIA, results in $0 < |\kappa| < 1$, maintaining a spin spiral ground state.

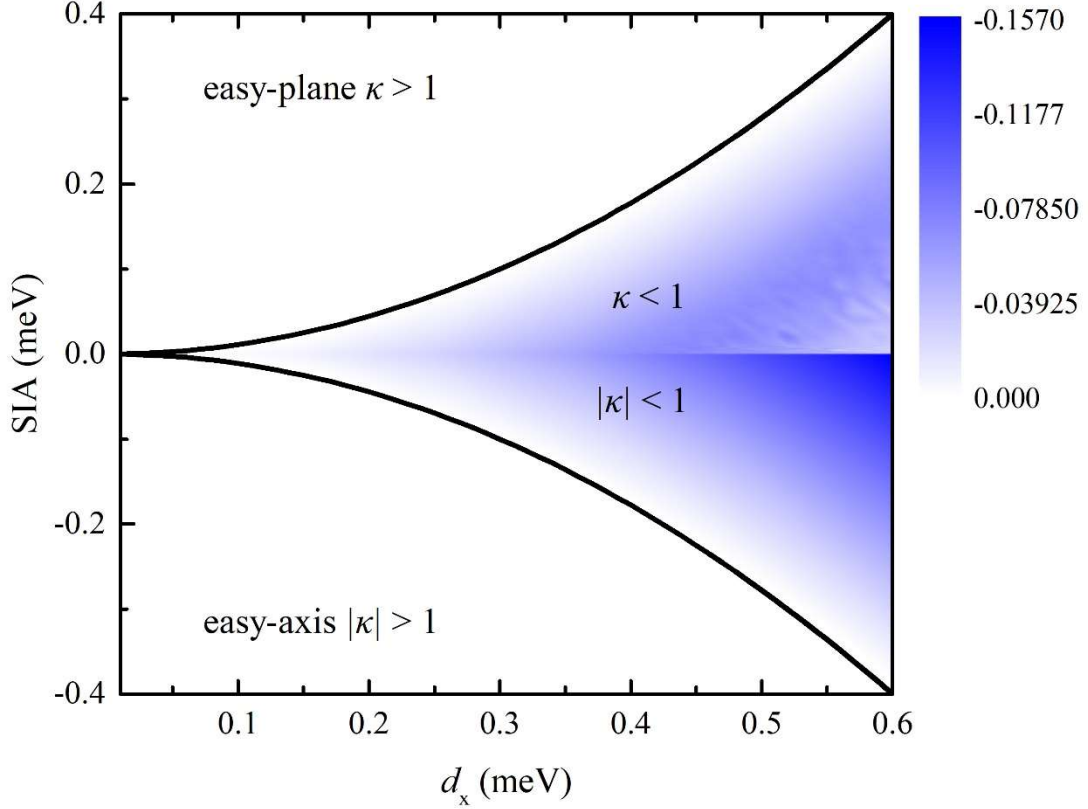


Figure 2. The d_x -SIA phase diagram at 0 K. The solid line denotes $|\kappa| = 1$. The energy difference between spin spiral and FM state is shown in the color bar.

To confirm the analysis provided above, by combining DFT calculations and the energy mapping method, we extract magnetic coefficients of monolayer $\text{Cr}_2\text{Ge}_2\text{Te}_6$, including Heisenberg exchange coupling J , DMI, and magnetocrystalline anisotropy (C-MAE). The first and second NN Heisenberg exchange coupling J_1 and J_2 is calculated to be 10.85 and -0.34 meV, respectively, which agree well with previous studies [34-36]. Due to the inversion symmetry, the first NN DMI is determined to be zero. In line with the aforementioned analysis, the second NN Cr pair does exhibit finite DMI. Specifically, for Cr_1 - Cr_2 pair as depicted in Figure 1, the planar component d_x is calculated to be 0.27 meV, the perpendicular component d_z is -0.61 meV, while the other planar component d_y is zero. Magnetic anisotropy energy (MAE) is also a crucial factor that influences the formation of topological spin texture. The MAE is composed of magnetocrystalline anisotropy energy (C-MAE) and magnetic dipolar anisotropy energy (D-MAE). The calculated C-MAE is 0.065 meV per Cr atom (prefers an out-of-plane magnetization), and the D-MAE is -0.039 meV per Cr atom (favors an in-plane magnetization). Thus, the total magnetic anisotropy energy is out-of-plane for

monolayer $\text{Cr}_2\text{Ge}_2\text{Te}_6$, which is also consistent with both theoretical and experimental works [37, 38].

After we obtained all the magnetic parameters, we now investigate the spin textures of monolayer $\text{Cr}_2\text{Ge}_2\text{Te}_6$ under different magnetic fields at 0 K. The spin Hamiltonian of Eq. (4) is used in PTMC simulations. For simplicity, both the C-MAE and D-MAE are included into the SIA. The PTMC simulations are also performed over a $60 \times 60 \times 1$ supercell. The initial spin configurations are obtained through fully relaxing the paramagnetic (random) state. To ensure the converged spin structures to be the ground state at 0 K, the conjugate gradient (CG) method is subsequently applied to relax the spin configurations obtained through PTMC simulations. Remarkably, without applying magnetic field, Bloch-type labyrinth domains are observed in monolayer $\text{Cr}_2\text{Ge}_2\text{Te}_6$ at 0 K, as depicted in Figure 3(a, c). For monolayer $\text{Cr}_2\text{Ge}_2\text{Te}_6$, the κ is determined to be 0.288, indicating a spin spiral ground state, which aligns closely with the results from PTMC simulations. Although there are many 2D magnetic materials that share the similar structure as $\text{Cr}_2\text{Ge}_2\text{Te}_6$, most of them exhibit collinear magnetic structure. Our phase diagram can explain this very well. It is known that $\text{Cr}_2\text{Si}_2\text{Te}_6$ is an FM insulator. Our calculated magnetic parameters lead to a κ value of 3.4, also suggesting FM ground state. Likewise, using the magnetic parameters available for monolayer CrI_3 [39], its κ is determined to be 10.7, indicating again FM ground state.

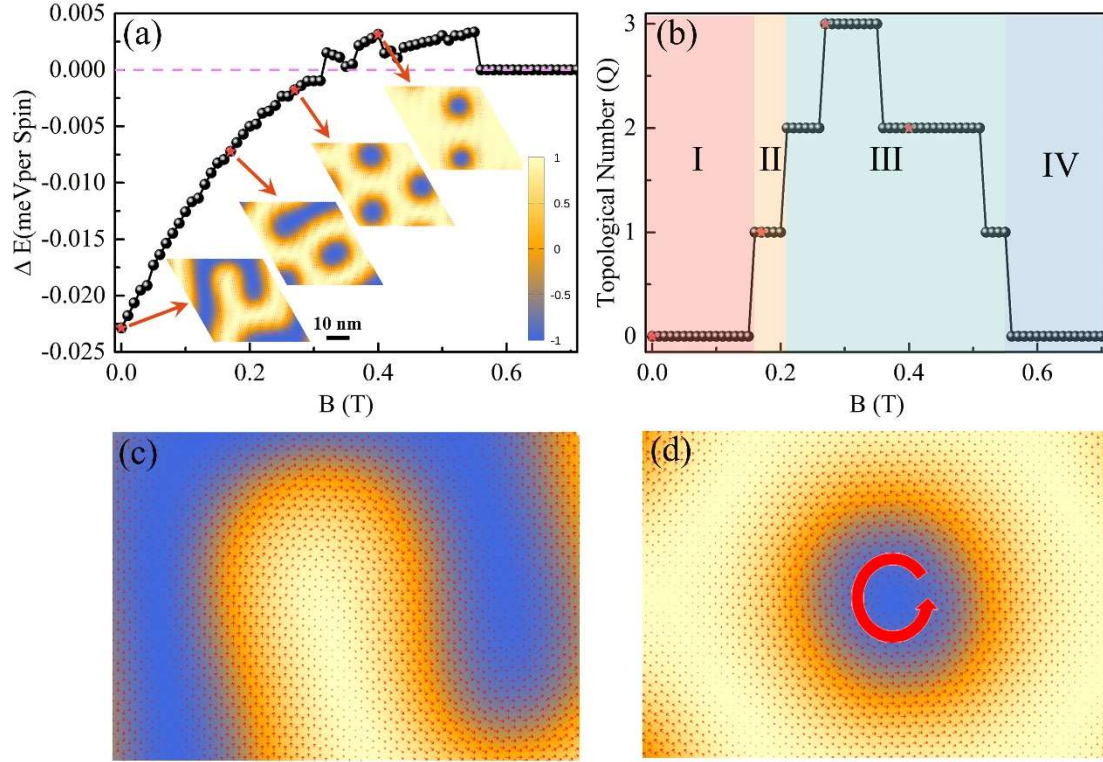


Figure 3. (a) The energy difference ΔE of $E(\text{relax})$ and $E(\text{FM-z})$ as a function of B at 0 K for monolayer $\text{Cr}_2\text{Ge}_2\text{Te}_6$. Here $E(\text{relax})$ is the energy obtained from CG method, $E(\text{FM-z})$ is the energy of FM state with magnetization lying along the z direction. The insets present the spin textures at different B . (b) The topological charge $|Q|$ as a function of B at 0 K. The phases found are as follows: labyrinth domains (I), labyrinths and skyrmion mixed phase (II), discrete skyrmions/skyrmions lattice (III), and saturated ferromagnetic state (IV), respectively. (c) and (d) are local view of spin textures in the insets of (a).

More intriguing, Bloch-type skyrmion is observed on the background of labyrinth domains at 0.17 T, as shown in Figure 3(a). The sense of in-plane spin rotation for both labyrinth domain and skyrmions are exactly consistent with the experimental observations [25, 27]. When the magnetic field is larger than 0.2 T, the labyrinth domains are totally wiped out. Importantly, as illustrated in Figure 3 (b), this skyrmion state is preserved within the range of 0.2-0.55 T. Above 0.55 T, the monolayer $\text{Cr}_2\text{Ge}_2\text{Te}_6$ is completely magnetized into the trivial ferromagnetic (FM) state. It should be noted that the skyrmions state is metastable within the field range of 0.31-0.55 T, which possesses a higher energy compared to the corresponding FM state. We note that Khela et al. [26] have also proposed that the second NN DMI plays a crucial role in the

formation of skyrmions in $\text{Cr}_2\text{Ge}_2\text{Te}_6$. However, in their atomistic spin dynamics simulations, three distinct types of topological spin texture are found: Bloch-type skyrmions and anti-skyrmions, and skyrmioniums. Importantly, the sense of in-plane spin rotation of the skyrmion identified in their simulations however contradicts the previous experimental results, which means the orientation of d_x component of second NN DMI used in their simulations is opposite to the direction derived from our DFT results.

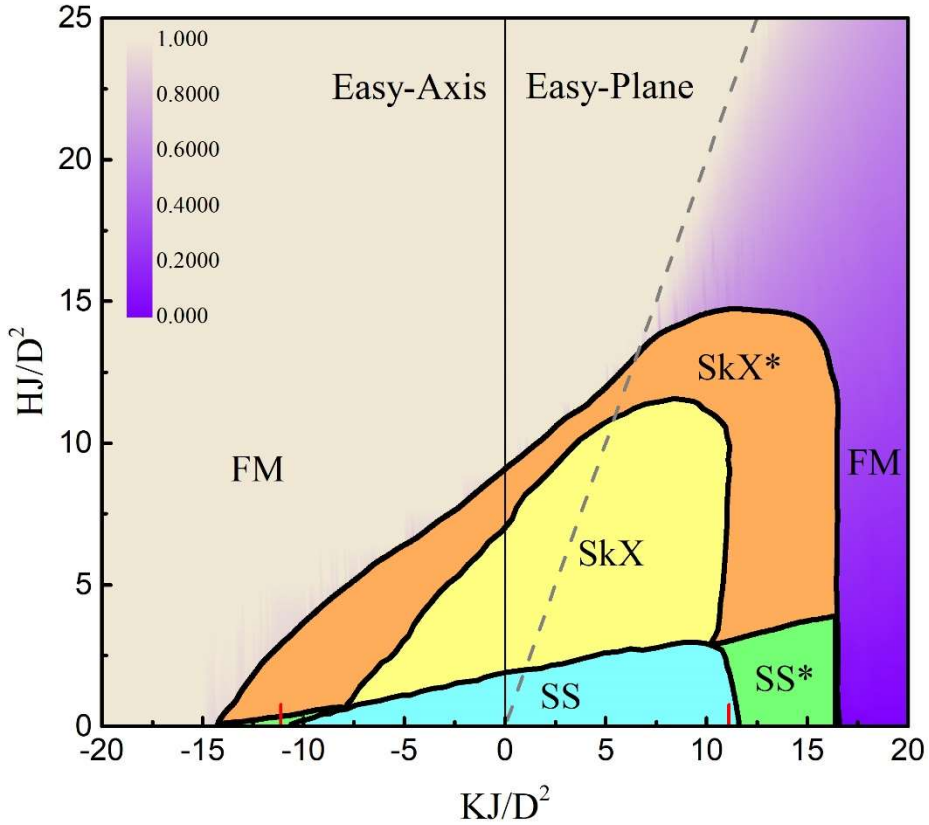


Figure 4. The SIA-field phase diagram with ferromagnetic (FM), spin spiral (SS), and skyrmion/skyrmions crystal (SkX) phases for $D = 0.3$ and $J = 10$ meV. The SS* and SkX* denotes the metastable spin spiral and skyrmion/skyrmions crystal (SkX) phase, respectively. The dashed line $H = 2A$ separates the out-of-plane FM from the tilted FM. For the FM, m^2 is shown in the color bar. The phase boundary is constructed based on magnetization (m^2), topological number, and energy difference between SS/SkX and the corresponding FM state, as a function of SIA and field. The red shot line indicates the boundary of $|\kappa| = 1$.

Finally, we establish anisotropy *versus* magnetic field phase diagram at 0K , as a function of dimensionless magnetic field HJ/D^2 and anisotropy KJ/D^2 , with fixed D (d_x)

$= 0.3$ and $J = 10$ meV, respectively. To construct the phase diagram (K, H) , we compare the energy of the states obtained by PTMC to that of the uniform (tilted) FM state, with the assistance of magnetization (m^z) and topological number. The uniform FM state can either be the spin polarized FM state along the magnetic field direction ($n_z = 1$) or the spin tilted FM state with $n_z < 1$. As shown in Figure 4, surprisingly, the easy-plane regime ($K > 0$) leads to an unexpectedly large stable SkX phase, compared to the easy-axis anisotropy ($K < 0$). This large region of the skyrmion/skyrmions crystal (SkX) within the phase diagram predominantly aligns around dashed line $H = 2A$ in Figure 4, marking the boundary between the "tilted FM" and the easy-axis FM. As demonstrated in the previous study [40, 41], this is due to: (i) the rotated spins within the skyrmion configuration reduce the DMI contribution to the free energy as compared to the FM state for easy-plane anisotropy; (ii) the skyrmion presents a more optimal balance between an easy-plane anisotropy and a field along the z-axis compared to a spiral configuration. Note that our PTMC calculations fail to give clear results near the phase boundaries because the system gets trapped in metastable states. Hence, the phase diagram depicted in Fig. 4 should be regarded only as semi-quantitative.

Summary

To summarize, we propose a mechanism that stabilize the skyrmions in centrosymmetric 2D magnets. Based the symmetry analysis, we ascertain that centrosymmetric 2D magnets with a honeycomb lattice do possess finite second NN DMI due to the broken local inversion symmetry. Our DFT and MC results well reproduce the spin spiral and skyrmions phases experimentally observed in $\text{Cr}_2\text{Ge}_2\text{Te}_6$, indicating the importance of the synergetic effect between the in-plane component (d_x) of the second NN DMI and the magnetic anisotropy. This unusual skyrmionics physics is revealed by introducing the dimensionless parameter κ , serving as determinants for non-collinear magnetic ground states. Furthermore, we present the anisotropy-field phase diagram, demonstrating that an in-plane anisotropy favors the formation of skyrmion states. Our results should serve as a guide for material parameters of 2D centrosymmetric magnets such that a large skyrmion region can be probed

experimentally.

Acknowledgments

This work is supported by the Natural Science Basic Research plan in Shaanxi Province of China (2022JQ-008, 2023-JC-YB-021), National Natural Science Foundation of China (No. 52172073), Open Foundation of Key Laboratory of Computational Physical Sciences (Ministry of Education), and Open Foundation of State Key Laboratory of Surface Physics and Department of Physics (KF2022_14). L.B. thanks the Vannevar Bush Faculty Fellowship Grant No. N00014-20-1-2834 from the Department of Defense and Award No. DMR-1906383 from the National Science Foundation Q-AMASE-i Program (MonArk NSF Quantum Foundry). Calculations were performed at the High-Performance Computing Center of Baoji University of Arts and Sciences.

Reference

1. Mühlbauer, S.; Binz, B.; Jonietz, F.; Pfleiderer, C.; Rosch, A.; Neubauer, A.; Georgii, R.; Boni, P. Skyrmion lattice in a chiral magnet. *Science* 2009, 323, 915–919.
2. Yu, X. Z.; Onose, Y.; Kanazawa, N.; Park, J. H.; Han, J. H.; Matsui, Y.; Nagaosa, N.; Tokura, Y. Real-space observation of a two-dimensional skyrmion crystal. *Nature* 2010, 465, 901–904.
3. Nagaosa, N.; Tokura, Y. Topological properties and dynamics of magnetic skyrmions. *Nat. Nanotechnol.* 2013, 8, 899.
4. Fert, A.; Reyren, N.; Cros, V. Magnetic skyrmions: advances in physics and potential applications. *Nat. Rev. Mater.* 2017, 2, 17031.
5. Kang, W.; Huang, Y.; Zhang, X.; Zhou, Y.; Zhao, W. Skyrmion-Electronics: An Overview and Outlook. *Proc. IEEE* 2016, 104, 2040–2061.
6. Yu, X. Z.; Kanazawa, N.; Onose, Y.; Kimoto, K.; Zhang, W. Z.; Ishiwata, S.; Matsui, Y.; Tokura, Y. Near room-temperature formation of a skyrmion crystal in thin-films of the helimagnet FeGe. *Nature Mater.* 10(2): 106-109 (2011).
7. Kézsmárki, I.; Bordács, S.; Milde, P.; Neuber, E.; Eng, L. M.; White, J. S.; Rønnow, H. M.; Dewhurst, C. D.; Mochizuki, M.; Yanai, K.; Nakamura, H.; Ehlers, D.; Tsurkan, V.; Loidl, A. Néel-type skyrmion lattice with confined orientation in the polar magnetic semiconductor GaV₄S₈. *Nature*

Mater. 14(11): 1116-1122 (2015).

8. Nayak, A. K.; Kumar, V.; Ma, T.; Werner, P.; Pippel, E.; Sahoo, R.; Damay, F.; Rößler, U. K.; Felser, C.; Parkin, S. S. P. Magnetic antiskyrmions above room temperature in tetragonal Heusler materials. *Nature*, 548(7669): 561-566 (2017).

9. Srivastava, A. K.; Devi, P.; Sharma, A. K.; Ma, T.; Deniz, H.; Meyerheim, H. L.; Felser, C.; Parkin, S. S. P. Observation of robust Néel skyrmions in metallic PtMnGa. *Adv. Mater.* 32(7): 1904327 (2020).

10. Kurumaji, T.; Nakajima, T.; Hirschberger, M.; Kikkawa, A.; Yamasaki, Y.; Sagayama, H.; Nakao, H.; Taguchi, Y.; Arima, T.-h.; Tokura, Y. Skyrmion Lattice With a Giant Topological Hall Effect in a Frustrated Triangular-Lattice Magnet. *Science* 2019, 365, 914–918

11. Hirschberger, M.; et al. Skyrmion Phase and Competing Magnetic Orders on a Breathing Kagomé Lattice. *Nat. Commun.* 2019, 10, 5831.

12. Takagi R, Matsuyama N, Ukleev V, et al. Square and rhombic lattices of magnetic skyrmions in a centrosymmetric binary compound. *Nature Communications*, 2022, 13(1): 1472.

13. Paddison J A M, Rai B K, May A F, et al. Magnetic Interactions of the Centrosymmetric Skyrmion Material Gd₂ PdSi₃. *Physical Review Letters*, 2022, 129(13): 137202.

14. Heinze, S.; von Bergmann, K.; Menzel, M.; Brede, J.; Kubetzka, A.; Wiesendanger, R.; Bihlmayer, G.; Blügel, S. Spontaneous atomic-scale magnetic skyrmion lattice in two dimensions. *Nat. Phys.* 7, 713–718 (2011).

15. Boulle, O.; et al. Room-temperature chiral magnetic skyrmions in ultrathin magnetic nanostructures. *Nature Nanotechnol.* 11(5): 449-454 (2016).

16. Woo, S.; et al. Observation of room-temperature magnetic skyrmions and their current-driven dynamics in ultrathin metallic ferromagnets. *Nature Mater.* 15(5): 501-506 (2016).

17. Moreau-Luchaire, C.; et al. Additive interfacial chiral interaction in multilayers for stabilization of small individual skyrmions at room temperature. *Nature Nanotechnol.* 11(5): 444-448 (2016).

18. Pollard, S. D.; Garlow, J. A.; Yu, J.; Wang, Z.; Zhu, Y.; Yang, H. Observation of stable Néel skyrmions in cobalt/palladium multilayers with Lorentz transmission electron microscopy. *Nature Commun.* 8(1): 1-8 (2017).

19. I. Dzyaloshinsky, A thermodynamic theory of “weak” ferromagnetism of antiferromagnetics, *J. Phys. Chem. Solids* 4, 241 (1958).

20. T. Moriya, Anisotropic superexchange interaction and weak ferromagnetism, *Phys. Rev.* 120, 91 (1960)
21. H. Yang, J. Liang, and Q. Cui, *Nat. Rev. Phys.* 5, 43 (2023)
22. Huang, B.; Clark, G.; Navarro-Moratalla, E.; Klein, D.; Cheng, R.; Seyler, K.; Zhong, D.; Schmidgall, E.; McGuire, M.; Cobden, D.; Yao, W.; Xiao, D.; Jarillo-Herrero, P.; Xu, X. Layer-dependent ferromagnetism in a van der Waals crystal down to the monolayer limit. *Nature* 2017, 546, 270–273.
23. Gong, C.; Li, L.; Li, Z.; Ji, H.; Stern, A.; Xia, Y.; Cao, T.; Bao, W.; Wang, C.; Wang, Y.; Qiu, Z. Q.; Cava, R. J.; Louie, S. G.; Xia, J.; Zhang, X. Discovery of intrinsic ferromagnetism in two-dimensional van der Waals crystals. *Nature* 2017, 546, 265–269.
24. Deng, Y.; Yu, Y.; Song, Y.; Zhang, J.; Wang, N. Z.; Sun, Z.; Yi, Y.; Wu, Y. Z.; Wu, S.; Zhu, J.; Wang, J.; Chen, X. H.; Zhang, Y. Gate-tunable room-temperature ferromagnetism in two-dimensional Fe₃GeTe₂. *Nature* 2018, 563, 94–99.
25. Han M G, Garlow J A, Liu Y, et al. Topological magnetic-spin textures in two-dimensional van der Waals Cr₂Ge₂Te₆. *Nano Letters*, 2019, 19(11): 7859-7865.
26. Khela M, Dąbrowski M, Khan S, et al. Laser-induced topological spin switching in a 2D van der Waals magnet. *Nature Communications*, 2023, 14(1): 1378.
27. McCray A R C, Li Y, Qian E, et al. Direct Observation of Magnetic Bubble Lattices and Magnetoelastic Effects in van der Waals Cr₂Ge₂Te₆. *Advanced Functional Materials*, 2023: 2214203.
28. Thomsen J D, Han M G, Penn A, et al. Magnetic Property Control of Cr₂Ge₂Te₆ Through Oxidation and Thickness Effects. *arXiv preprint arXiv:2310.02319*, 2023.
29. Vervelaki A, Bagani K, Jetter D, et al. Visualizing thickness-dependent magnetic textures in few-layer Cr₂Ge₂Te₆. *arXiv preprint arXiv:2311.08529*, 2023.
30. Tran H B, Matsushita Y. Skyrmions in van der Waals centrosymmetric materials with Dzyaloshinskii–Moriya interactions. *Scripta Materialia*, 2024, 239: 115799.
31. Fert, A., Cros, V., Sampaio, J. Skyrmions on the track. *Nature Nanotechnol.*, 8(3): 152-156 (2013).
32. B. Schweflinghaus, B. Zimmermann, M. Heide, G. Bihlmayer, and S. Blügel, *Phys. Rev. B* 94, 024403 (2016).
33. B. Zimmermann, G. Bihlmayer, M. Böttcher, M. Bouhassoune, S. Lounis, J. Sinova, S. Heinze,

- S. Blügel, and B. Dupé, Comparison of first-principles methods to extract magnetic parameters in ultrathin films: Co/Pt(111), *Phys. Rev. B* 99, 214426 (2019).
34. Y. M. Fang, S. Q. Wu, Z. Z. Zhu, and G. Y. Guo, *Phys. Rev. B* 98, 125416 (2018)
35. Z. L. Li, T. Cao, and S. G. Louie, *J. Magn. Magn. Mater.* 463, 28 (2018)
36. Zhang B H, Hou Y S, Wang Z, Wu R. Q. First-principles studies of spin-phonon coupling in monolayer Cr₂Ge₂Te₆. *Physical Review B*, 2019, 100(22): 224427.
37. C. Gong, L. Li, Z. Li, H. Ji, A. Stern, Y. Xia, T. Cao, W. Bao, C. Wang, Y. Wang, Z. Q. Qiu, R. J. Cava, S. G. Louie, J. Xia, X. Zhang, Discovery of intrinsic ferromagnetism in two-dimensional van der Waals crystals. *Nature* 546, 265–269 (2017).
38. Zhu F, Zhang L, Wang X, et al. Topological magnon insulators in two-dimensional van der Waals ferromagnets CrSiTe₃ and CrGeTe₃: Toward intrinsic gap-tunability. *Science advances*, 2021, 7(37): eabi7532.
39. Xu, C., Feng, J., Prokhorenko, S., Nahas, Y., Xiang, H., Bellaiche, L. Topological spin texture in Janus monolayers of the chromium trihalides Cr(I, X)₃. *Phys. Rev. B* 101, 060404 (2020).
40. Banerjee, S., Rowland, J., Erten, O., Randeria, M. Enhanced stability of skyrmions in two-dimensional chiral magnets with Rashba spin-orbit coupling. *Phys. Rev. X*, 4(3), 031045 (2014).
41. U. Güngördü, R. Nepal, O. A. Tretiakov, K. Belashchenko, and A. A. Kovalev, Stability of skyrmion lattices and symmetries of quasi-two-dimensional chiral magnets, *Phys. Rev. B* 93, 064428 (2016)